



# Hydrophobic@amphiphilic hybrid nanostructure of iron-oxide and graphene quantum dot surfactant as a theranostic platform

Sepand Tehrani Fateh<sup>a,b</sup>, Mahdieh Ahmadi Kamalabadi<sup>c</sup>, Azita Aliakbari<sup>d</sup>,  
Saeideh Jafarnejad-Farsangi<sup>e</sup>, Maedeh Koochi<sup>f</sup>, Elham Jafari<sup>g</sup>, Zahra Miri Karam<sup>h</sup>,  
Fariborz Keyhanfar<sup>i,\*</sup>, Amin Shiralizadeh Dezfuli<sup>b,j,\*</sup>

<sup>a</sup> School of Medicine, Shahid Beheshti University of Medical Sciences (SBMU), Tehran, Iran

<sup>b</sup> Ronash Technology Pars Company, Tehran, Iran

<sup>c</sup> Non-Communicable Diseases Research Center, Rafsanjan University of Medical Sciences, Rafsanjan, Iran

<sup>d</sup> Department of Biology, Faculty of Life Sciences, Tonekabon Branch, Islamic Azad University, Mazandaran, Iran

<sup>e</sup> Physiology Research Center, Institute of Neuropharmacology, Kerman University of Medical Sciences, Kerman, Iran

<sup>f</sup> Department of Chemistry, Faculty of Science, University of Zanjan, Zanjan, Iran

<sup>g</sup> Department of Pathology, Pathology and Stem Cell Research Center, Kerman University of Medical Sciences, Kerman, Iran

<sup>h</sup> Cardiovascular Research Center, Institute of Neuropharmacology, Kerman University of Medical Sciences, Kerman, Iran

<sup>i</sup> Department of Pharmacology, Faculty of Medicine, Iran University of Medical Sciences (IUMS), Tehran, Iran

<sup>j</sup> Radiation Biology Research Center, Iran University of Medical Sciences (IUMS), Tehran, Iran

## ARTICLE INFO

### Keywords:

Theranostics  
Magnetic nanoparticles  
Graphene quantum dots  
Surfactant  
Hybrid nanomaterials

## ABSTRACT

Nanostructure hybrids offer exceptional properties and multifunctionality, suitable for the field of theranostics. Graphene quantum dots (GQDs) and magnetic nanoparticles (MNPs) are two possible candidates to be used these hybrids due to their chemical, physical and biological properties. GQDs can be modified to act as surfactants. In this study, a hybrid nanostructure of GQDs and MNP has been synthesized based on hydrophobic interactions between long carbon chains on the surface of GQDs on the surroundings and MNP at the center. We have synthesized GQDs through a pyrolysis process and modified them with cetyl alcohol to obtain a surfactant-GQDs (CAGQDs). Moreover, Iron-oxide nanoparticles (IONP) as MNP has been synthesized using oleate-iron complex. Afterward, CAGQDs and IONP are hybridized, leading to a structure in which IONP is located at the center, and it is surrounded by CAGQDs (IONP@CAGQD). IONP@CAGQD possesses fluorescent and magnetic properties. Moreover, hydrophobic and hydrophilic cargo loading abilities, contrast enhancement, targeting abilities, and stimuli-responsiveness are other features of this structure. Furthermore, Low cytotoxicity of IONP@CAGQD makes its biomedical applications possible. IONP@CAGQD can potentially be used as a multifunctional theranostic agent.

## 1. Introduction

Nanostructures are suitable candidates for theranostic purposes due to their small size, functionalization potentials, penetration abilities, biocompatibility, and multifunctionality. An efficient theranostic nano-platform needs to be stable enough, possess superior

\* Corresponding authors at: Ronash Technology Pars Company, Tehran, Iran.

E-mail address: [amindezfuli@outlook.com](mailto:amindezfuli@outlook.com) (A. Shiralizadeh Dezfuli).

<https://doi.org/10.1016/j.onano.2022.100037>

Received 10 December 2021; Received in revised form 10 March 2022; Accepted 14 March 2022

Available online 15 March 2022

2352-9520/© 2022 Published by Elsevier Inc. This is an open access article under the CC BY-NC-ND license (<http://creativecommons.org/licenses/by-nc-nd/4.0/>).

cargo-loading and -releasing profile, and make imaging or diagnostic applications possible. Hybridization of different nanoparticles would lead to the accumulation of various chemical, physical and biological features, all in one single complex [1,2].

GQDs and Metal nanoparticles are among the most frequently used nanoparticles in biomedical applications [3,4]. Moreover, hybrid nanoparticles consisted of both GQDs and Metal nanoparticles are being fabricated and studied extensively. Bacon et al. have defined GQDs as “graphene fragments that are small enough to cause exciton confinement and a quantum size effect” [5]. Partial pyrolysis of organic materials, including sugar, polythiophene, and citric acid, is among several GQDs synthesis methods [3]. GQDs have been utilized in different biomedical applications due to their unique physical and chemical properties [3]. GQD fluorescence stability would make biological imaging more efficient. Moreover, GQDs can be loaded with desired drugs through  $\pi$ - $\pi$  interactions between GQDs and loaded drugs. Besides, various functional groups on the surface or edges of GQDs would make functionalization and surface modification of GQDs possible [3,6]. The addition of other nanoparticles, such as magnetic nanoparticles to GQDs, would lead to more multifunctional complexes for biomedical applications. Magnetic nanoparticles are typically classified into pure metals, metal oxides, and magnetic nanocomposites, and iron oxide NPs (typically  $\text{Fe}_2\text{O}_3$  or  $\text{Fe}_3\text{O}_4$ ) are the most frequently used magnetic nanoparticles [7]. Magnetic nanoparticles are being used as contrast agents in both MRI and Computed tomography (CT) scan. Moreover, magnetic separation, targeted drug delivery, hyperthermia therapy, and thermo-ablation, and bio-sensing are other possible applications of these nanoparticles [4].

GQDs can also be modified to act as surfactants. Surfactants play a critical role in many chemical processes, biomedical applications, and nanostructures' formation and function [8]. Adding different components including hexylamine, oleylamine, dodecylamine, and Sodium laurate to GQDs or its carboxylation would generate amphiphilic properties that make GQDs a potential surfactant [8–12]. It has been demonstrated that GQDs-surfactants may possess high emulsification efficiency, low production cost, uniform morphology, photoluminescence properties, and high stability [13].

Herein, we have fabricated a GQDs-surfactant using cetyl alcohol (CA) and then propose a novel hybrid structure of GQDs-surfactant and MNPs, which are brought together by hydrophobic interaction between the intermediary long carbon chains attached on both GQDs and MNPs.

## 2. Materials and method

### 2.1. Synthesis of $\text{Fe}_3\text{O}_4$ MNPs (IONP)

IONP have been synthesized through the thermal decomposition method using the oleate-iron complex [14]. For this purpose, 8 mmol of iron nitrate ( $\text{Fe}(\text{NO}_3)_3 \cdot 9\text{H}_2\text{O}$ , 98%) in addition to 24 mmol of sodium oleate (95%) were added to a solvent with the following composition: 12 ml of water, 16 ml of ethanol, and 28 ml of hexane. Afterward, this solution was heated at 70 °C for 4 h. Then the synthesized product was washed several times using water and then dried in a vacuum oven at 60 °C for 4 h.

### 2.2. Synthesis of CAGQD

In a typical procedure of GQDs preparation through pyrolysis, 1 gr citric acid was placed in the oil bath at 190 °C for 5 min, which makes citric acid melted and discolored [15]. Afterward, 0.1 gr of CA was added to the reaction chamber. During 30 min, the color of the mentioned liquid was darkened from colorless to yellow and orange, indicating the formation of CAGQDs.

### 2.3. Hybridization of IONP@CAGQD

To hybridize pre-synthesized IONP and CAGQD with each other, 0.005 g of IONP was dispersed in a solution containing 12 ml of 99.9% toluene and 3.5 ml of 96% alcohol, and then it was sonicated for 5 h. Afterward, 5 ml of prepared IONP solution was added to 0.5 g melted CAGQD. After 10 min, a two-phase liquid was formed, and after 30 min of stirring, the synthesized nanoparticle hybrids entered the lower phase of the liquid and left the toluene on the top.

### 2.4. Cell culture

Mouse embryonic fibroblast 3T3 cells, Human umbilical vein endothelial cells (HUVEC), and human breast tumor MCF-7 cells were purchased from the Pasteur Institute of Iran (Tehran, Iran). Dulbecco modified Eagle's medium (DMEM) was used for 3T3 cells, and DMEM/F12 media was used for HUVEC and MCF-7 cells. Culture media was supplemented with 10% fetal bovine serum (FBS) and 2% streptomycin and penicillin. All cells were incubated at 37 °C under 5%  $\text{CO}_2$  and 85% humidity conditions.

### 2.5. In vitro cell viability assessment

MTT (3-(4,5-dimethylthiazol-2-yl)-2,5-diphenyltetrazolium bromide) method was used for the assessment of cell viability. Cells were cultured at a density of  $1 \times 10^4$  cells per well in 96 well plates. When cultured cells reached the density of 80%, the media was removed, and cells were exposed to different concentrations (2000–1.95  $\mu\text{g}\cdot\text{mL}^{-1}$ ) of CAGQD and IONP@CAGQD for 24 h. Then, the media was removed and replaced with MTT solution (5  $\text{mg}\cdot\text{mL}^{-1}$ ) for 3 h. After that MTT was removed and replaced with 90  $\mu\text{L}$  DMSO (dimethyl sulfoxide) for 30 min. Viable cells reduce tetrazolium salt to formazan, which is purple and it can be quantified by measuring the absorbance at 590 nm. Finally, % viability of cells was calculated according to the following formula:

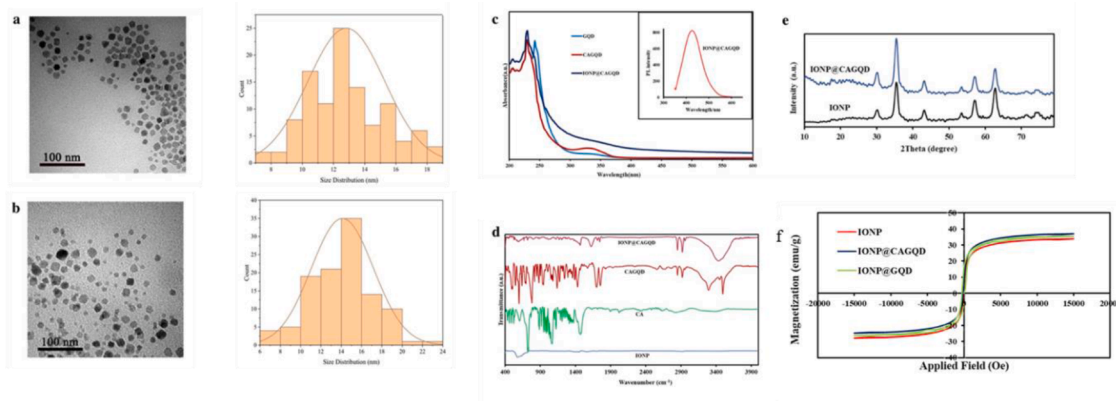


**Fig. 1.** Characterization of GQDs, CAGQDs, IONP, and IONP@CAGQDs. (a, b) TEM image of IONP and IONP@CAGQD respectively, (c) UV analysis results of GQD, CAGQD, and IONP@CAGQD, (d) FT-IR analysis results of IONP, CA, CAGQD, (e) XRD analysis results of IONP, and IONP@CAGQD, and IONP@CAGQD, (f) Magnetization hysteresis loops results of IONP and IONP@CAGQD.

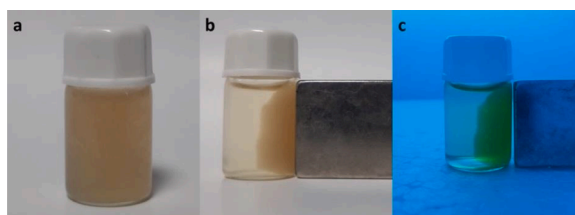


**Fig. 2.** Photograph of Fluorescence and magnetic properties of IONP@CAGQD. (a) Gross appearance of stable IONP@CAGQD, (b) accumulation of IONP@CAGQD in a magnetic field applied by a magnet, (c) Fluorescent emission of IONP@CAGQD under UV light.

$$\text{Cell Viability (\%)} = \frac{\text{Absorbance of samples}}{\text{Absorbance of Control}} \times 100$$

## 2.6. Animal study

BALB/c mice weighted 30 gr were housed in an animal room (Physiology Research Center, Kerman, Iran) under standard conditions, including free access to water and food, 12/12 h light/dark cycle at  $21 \pm 2$  °C. All experiments were performed according to the national guidelines for animal studies. Forty mice divided into eight groups ( $n = 5$ ): Controls, IONP@CAGQD 1 mg.Kg<sup>-1</sup> for 1 day, IONP@CAGQD 3 mg.Kg<sup>-1</sup> for 1 day, IONP@CAGQD 6 mg.Kg<sup>-1</sup> for 1 day, IONP@CAGQD 1 mg.Kg<sup>-1</sup> for 7 days, IONP@CAGQD 3 mg.Kg<sup>-1</sup> for 7 days, IONP@CAGQD 6 mg.Kg<sup>-1</sup> for 7 days.

## 2.7. Hematoxylin and eosin staining

Liver and heart tissues were fixed in formaldehyde solution (4% v/v), and 5  $\mu$ m-thickness sections were prepared from paraffin-embedded blocks and stained with Hematoxylin and eosin (H&E) and Perls' Prussian blue stains to examine the general microscopic features of tissues and assessment of non-heme iron deposition, respectively. All histological sections were carefully reviewed in a blinded fashion by an experienced pathologist under light microscopy.

Iron deposition, muscular hypertrophy, and fibrosis in heart tissue were scored in respect to location and intensity using a relative scale from 0 to 4 [16]. Histological assessment of liver tissue was performed considering hydropic degeneration, necrosis and inflammation and scored according to Wood et al [16]. Iron deposition in liver tissue was assessed separately in the sinusoidal cells and hepatocytes [16,17].

## 2.8. Instrumentation

X-ray powder diffraction (XRD) patterns were obtained by a Rigaku D-max C III XRD using a Ni-filtered Cu K $\alpha$  radiation Field. The Fourier transform infrared (FTIR) spectra were obtained via an FT-IR spectrophotometer (Thermo Nicolet 360). UV-Vis analysis was measured by a UV-Vis spectrophotometer (Lambda 750). Magnetic studies were performed in a vibrating sample magnetometer (VSM) (BHV-55, Riken, Japan) at room temperature. Imaging of the structures was done by a Transmission Electron Microscope (TEM) (Philips EM430 ST). Evaluation of tissues was done through light microscopy (Olympus System Microscope Model CX33). The

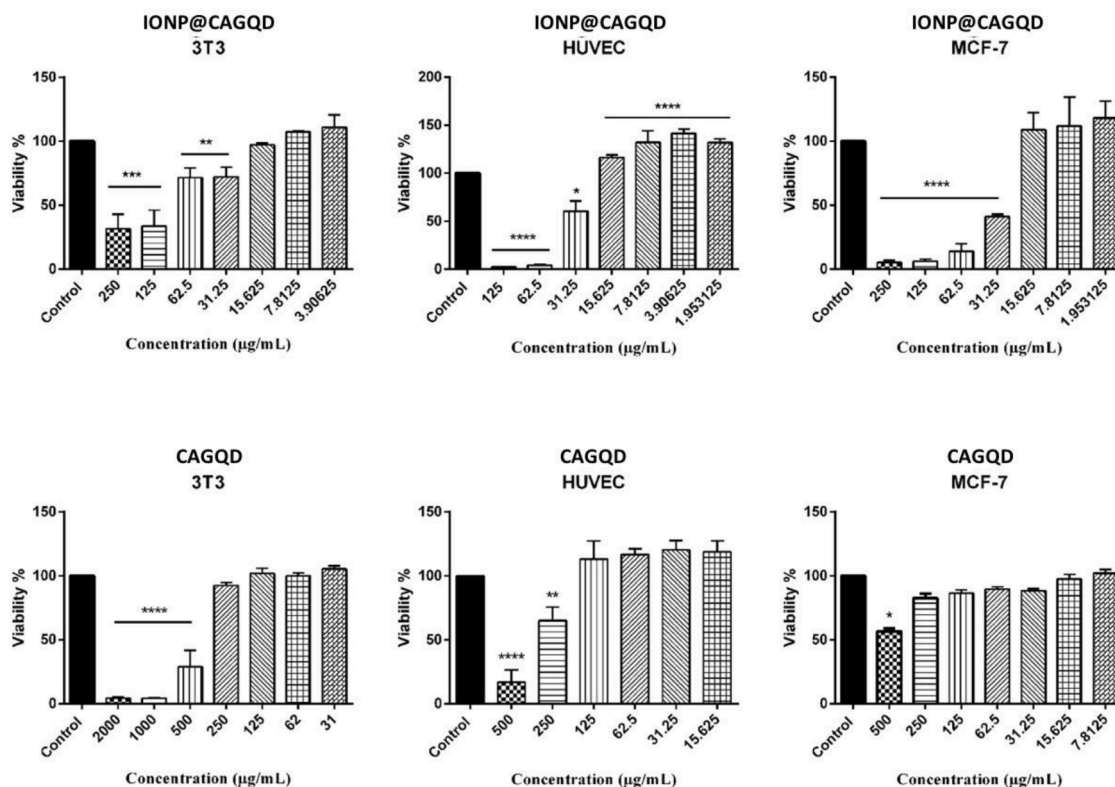


**Fig. 3.** *In vitro* viability of the cells. Viability of 3T3 fibroblasts, HUVEC and MCF-7 cells were exposed to different concentrations of IONP@CAGQD (A) and CAGQD (B) for 24 h. \*  $P < 0.05$ , \*\*  $P < 0.01$ , \*\*\*  $P < 0.001$ , \*\*\*\*  $P < 0.0001$ .

absorbance of samples for cell viability analysis was measured by a microplate reader (Bio-Tec ELX800, USA)

### 3. Result and discussion

#### 3.1. Characterization

Fig. 2 TEM image have shown well-dispersed IONP and IONP@CAGQD particles sizing 10–12 nm and 13–16 nm, respectively, which are confirmed by size distribution analysis (Fig. 1a and b). Moreover, the distribution of the particles' size is relatively concentrated and uniform. UV-vis analysis of GQD has shown a strong absorbance at 340 nm (Lambda Max=0.166) (Fig. 1c). CAGQD possesses a strong absorbance at 338 (Lambda Max=0.322) (Fig. 1c). The change in the maximum absorption is related to the strong bond between CA and GQD. The highest absorbance for IONP@CAGQD can be seen at 336 nm (Lambda Max=0.582), which is due to the conjugation of CAGQD with IONP (Fig. 1c) [15]. Symmetric and asymmetric tensile vibrations in the area of  $1637\text{cm}^{-1}$  and  $1560\text{cm}^{-1}$  are related to the water transfer (Fig. 1c) [15]. FT-IR analysis of IONP demonstrates a peak around  $576\text{cm}^{-1}$ , which indicates the presence of Fe-O. For hydrophilic nanoparticles, the peak related to C-O single-bond stretching of the carboxylic group can be seen around  $1051\text{cm}^{-1}$ , and the peaks related to the symmetrical and asymmetrical stretching vibration of carboxylic acid group oleic acid can be seen around  $1512\text{cm}^{-1}$  and  $1412\text{cm}^{-1}$ , respectively. The peak around  $3400\text{cm}^{-1}$  indicates OH functional group. The peaks around  $2852\text{cm}^{-1}$  and  $2921\text{cm}^{-1}$  are related to symmetrical and asymmetrical vibrations of  $\text{CH}_2$  of the alkyl chain. Three peaks at  $1464\text{cm}^{-1}$ ,  $1063\text{cm}^{-1}$ , and  $719\text{cm}^{-1}$  are attributed to the CA. The FT-IR analysis for CAGQD demonstrates a peak related to CH stretching vibration at  $2950\text{cm}^{-1}$ . Moreover, CA-attributed peaks are also present. The FT-IR analysis for IONP@CAGQD demonstrates a peak at  $3400\text{cm}^{-1}$ , related to the OH, and two peaks at  $2852\text{cm}^{-1}$  and  $2921\text{cm}^{-1}$  related to symmetrical and asymmetrical vibrations of the CH group. Moreover, the stretching vibrations attributed to CH are decreased significantly. Two peaks can be seen at  $1512\text{cm}^{-1}$  and  $1412\text{cm}^{-1}$ , which indicates the symmetrical and asymmetrical stretching vibrations of Carboxylic acid groups of oleic acids. The peaks at  $576\text{cm}^{-1}$  in both results are attributed to Fe. In addition, CA-attributed peaks can be seen. FT-IR analysis results can be seen in Fig. 1d. XRD analyses of IONP and IONP@CAGQD demonstrate several peaks at (220), (311), (400), (422), (440), and (511), which are consistent with the JCPDS card (65-3107) pattern (Fig. 1e). The average size of crystals for IONP and IONP@CAGQD is calculated to be 11–13 nm and 13–15 nm, respectively [14] Magnetization hysteresis loops have been measured for IONP and IONP@CAGQD through a sweeping external magnetic field at room temperature. No coercivity or remanence indicating super-paramagnetism properties have been observed. The  $M_s$  Values for IONP and IONP@CAGQD have been calculated to be  $34.1\text{ emu/g}$  and  $37.8\text{ emu/g}$  (Fig. 1f). The slight

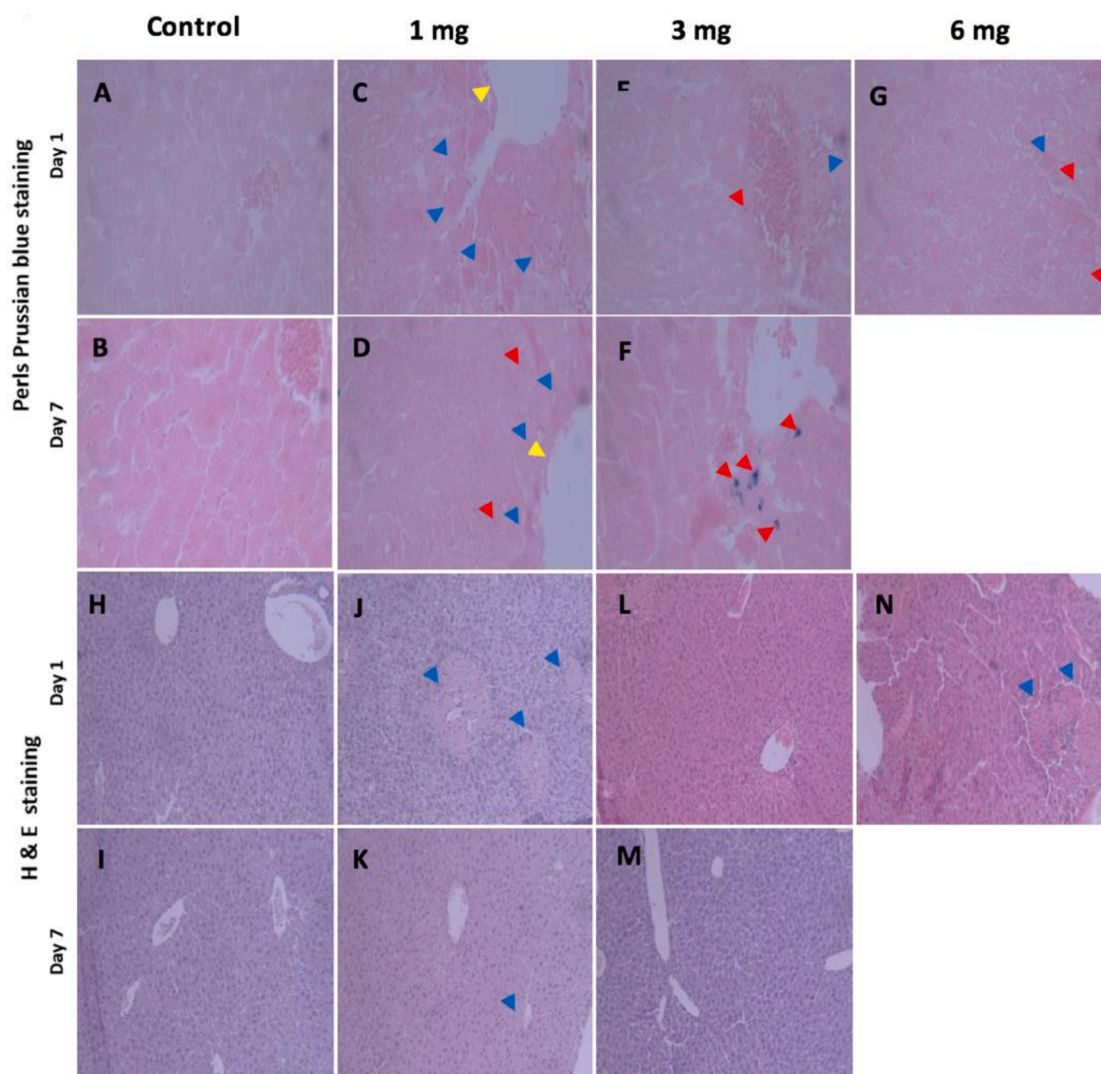


**Fig. 4.** Iron deposition (Perls Prussian blue stain) and Histopathology (H and E) of the liver. Mice were treated with 1, 3, and 6 mg.Kg<sup>-1</sup> of MN@GQD, and iron deposition (A–G) and pathological changes (H–N) in the liver were investigated 1 and 7 days after treatments. According to Perls Prussian blue staining images (A–G), no evidence of iron deposition was observed in the control groups (A, B). No evidence of Iron deposition, instead extensive necrotic areas around central veins was observed (C). Slight iron deposits in hepatocytes (grade 1 (D, G); grade 2 (E); grade 4 (F)) and reticuloendothelial cells (F) with bright blue in color, and few necrotic hepatocytes around central veins (zone 3) (D and E) were detected. According to H & E staining images (H–N), liver tissue with preserved architecture was observed in the control group (H, I). Extensive necrosis of liver cells around the central vein and hydropic degeneration of hepatocytes was detected (J). The preserved architecture of the liver tissue without necrotic areas (M) was observed seven days after 3 mg.Kg<sup>-1</sup> injection of MN@GQD. All mice were dead in groups treated with 6 mg.Kg<sup>-1</sup> of IONP@CAGQD for 7 days. The magnification was 400X (A–G) and 100X (H–M). Red arrows: Iron deposition; Central veins: (Yellow arrows); necrotic areas: (Blue arrows). Zone 3: area occupied by hepatocytes immediately around the central veins. A and H: Controls for 1 day; B and I: controls for 7 days; C and J: 1 mg.Kg<sup>-1</sup> IONP@CAGQD for 1 day; D and K: 1 mg.Kg<sup>-1</sup> IONP@CAGQD for 7 days; E and L: 3 mg.Kg<sup>-1</sup> IONP@CAGQD for 1 day; F and M: 3 mg.Kg<sup>-1</sup> IONP@CAGQD for 7 days; G and N: 6 mg.Kg<sup>-1</sup> IONP@CAGQD for 1 day (For interpretation of the references to color in this figure legend, the reader is referred to the web version of this article.).

increase in the magnetism of IONP@CAGQD in comparison with IONP can be attributed to an increase in the effective weight of the final nanoparticle after the reaction between two sub-components. According to VSM analysis, the presence of cetyl alcohol has almost no effect on magnetic properties.

### 3.2. *In vitro* viability of the cells

MTT assay is a fast and colorimetric method to quantify live cells according to metabolic activity. We exposed two normal (3T3 and HUVEC) and one cancerous (MCF-7) cell line to CAGQD and IONP@CAGQD. We observed that the toxicity of CAGQD was less than

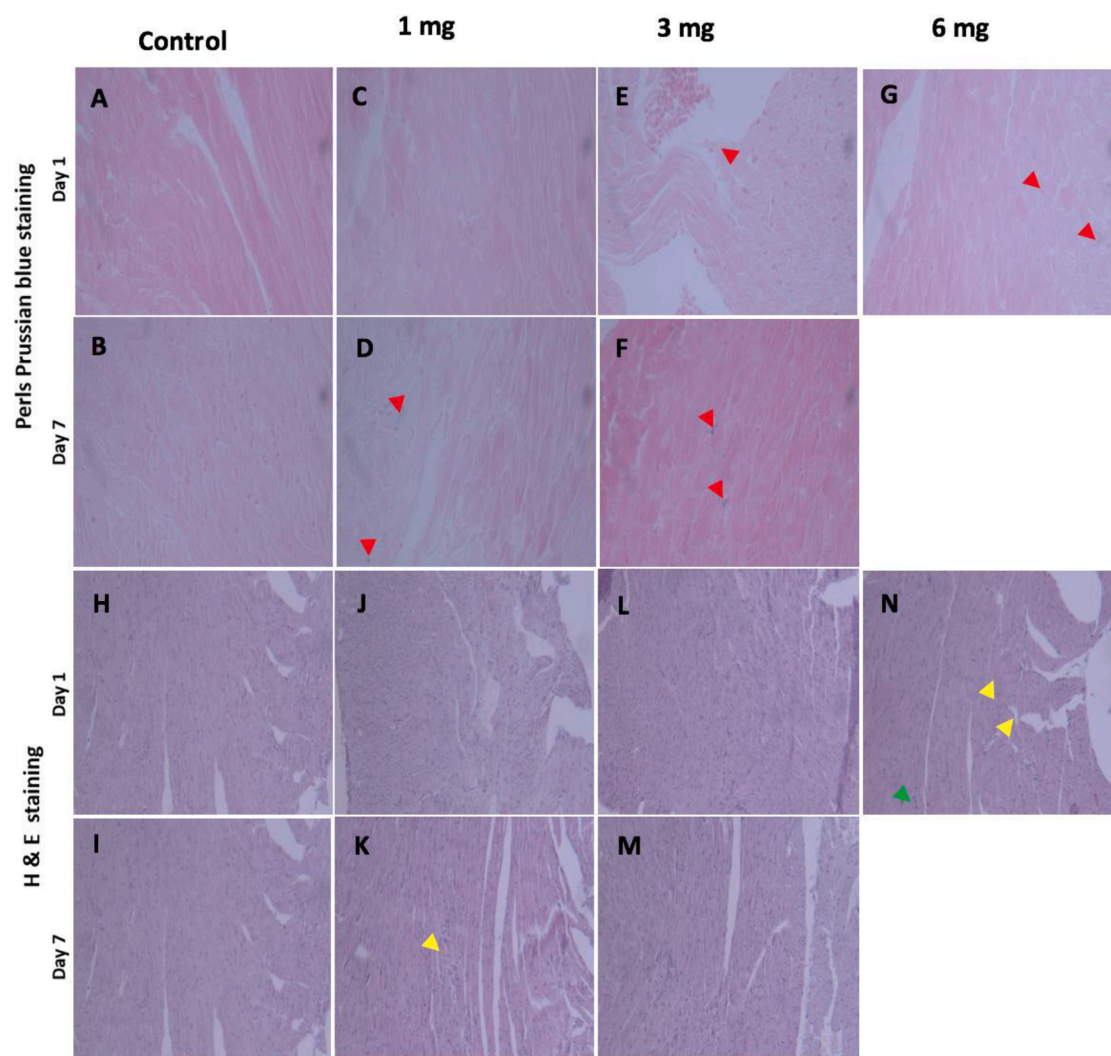


**Fig. 5.** Iron deposition (Perls Prussian blue stain) and Histopathology (H and E) of the heart. Mice were treated with 1, 3, and 6 mg Kg<sup>-1</sup> of MN@GQD, and iron deposition (A–G) and pathology changes (H–N) in the heart were investigated 1 and 7 days after treatments. According to Perls Prussian blue staining images (A–G), no evidence of iron deposition was observed in the controls (A, B) and mice treated with 1 mg.Kg<sup>-1</sup> for one day (C). Slight (score 1) (D, E, G) or mild (score 2) (F) iron deposition located in the interstitial and endothelial cells was observed. According to H & E staining images (H–N), heart tissue with a normal appearance was observed in the control groups (H and I). Mild (J–M) and extensive (N) edema and vascular congestion detected with small foci of mononuclear inflammatory cells (N). All mice were dead in groups treated with 6 mg.Kg<sup>-1</sup> of IONP@CAGQD for 7 days. Original magnification: x400 (A–G) and x100 (H–N). Red arrows: iron deposition; Yellow arrows: edema and vascular congestion; Green arrows: necrotic areas. A and H: Controls for 1 day; B and I: controls for 7 days; C and J: 1 mg.Kg<sup>-1</sup> IONP@CAGQD for 1 day; D and K: 1 mg.Kg<sup>-1</sup> IONP@CAGQD for 7 days; E and L: 3 mg.Kg<sup>-1</sup> IONP@CAGQD for 1 day; F and M: 3 mg.Kg<sup>-1</sup> IONP@CAGQD for 7 days; G and N: 6 mg.Kg<sup>-1</sup> IONP@CAGQD for 1 day (For interpretation of the references to color in this figure legend, the reader is referred to the web version of this article).

IONP@CAGQD, and all cell lines were alive at the concentration of 250 µg.mL<sup>-1</sup>. The concentration of IONP@CAGQD at which 50% of cells were alive (IC50) was 47, 48, and 17.56 µg.mL<sup>-1</sup> for 3T3, HUVEC, and MCF-7 cells, respectively. It seems that IONP@CAGQD is more toxic for tumor cells in comparison with normal cells (Fig. 3). However, both compounds demonstrated acceptable biocompatibility for biomedical applications.

### 3.3. Animal and histological study

To investigate *in vivo* toxicity, IONP@CAGQD was injected intravenously into mice at three (1, 3, and 6 mg Kg<sup>-1</sup>) concentrations, and histopathological changes and non-hem iron deposition in liver and cardiac tissues were evaluated 1 and 7 days after injection. Since the liver is the main destination for aggregation and degradation of about 30 to 99% of injected nanoparticles [18], this organ would, as well, reflect the toxicity situation. According to H & E results, we observed hydropic degeneration and necrotic areas,

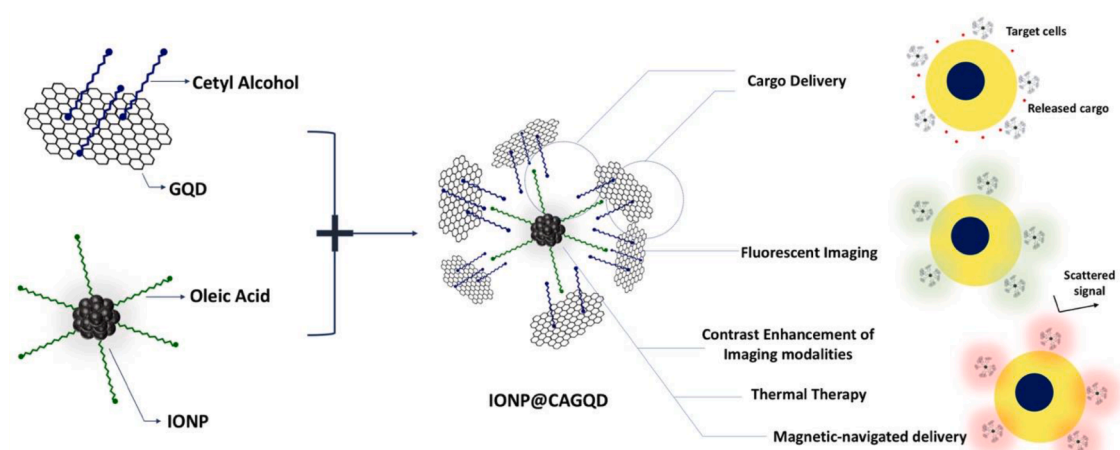


Fig. 6. Schematic illustration of IONP@CAGQD and its applications.

especially around the central veins in all groups that received IONP@CAGQD (Fig. 4I, J, L, M) except in IONP@CAGQD  $3 \text{ mg.Kg}^{-1}$  for 7 days (Fig. 4K). The architecture of the liver tissue was preserved without necrotic areas in this group. The most extensive necrotic areas were observed in the liver received  $1 \text{ mg.Kg}^{-1}$  of IONP@CAGQD for 1 day. Interestingly, necrotic hepatocytes around central veins decreased after 7 days. It should be noted that all mice who died in the group that received  $6 \text{ mg.Kg}^{-1}$  for 7 days. According to Perls Prussian blue staining results (Fig. 4A–G), all groups that received IONP@CAGQD showed the presence of iron deposition except IONP@CAGQD  $1 \text{ mg.Kg}^{-1}$  for 1 day (Fig. 4C). Collectively, administration of  $3 \text{ mg.Kg}^{-1}$  for 7 days had the less toxic effect on the liver and  $1 \text{ mg.Kg}^{-1}$  for 1 day and  $6 \text{ mg.Kg}^{-1}$  for 7 days showed the most toxic effect on the liver.

In addition to the liver tissue, the toxicity of IONP@CAGQD was evaluated in heart tissue as a target organ for drug delivery in nanomedicine. According to H & E results (Fig. 5H–N), cardiac tissue in mice received  $6 \text{ mg.Kg}^{-1}$  of IONP@CAGQD for one day (Fig. 5N) showed extensive edema, vascular congestion, and small foci of mononuclear inflammatory cells in comparison with the control (Fig. 5H). Other groups showed mild edema and vascular congestion in comparison with the control. According to Perls Prussian blue staining results (Fig. 5A–G). All groups showed the presence of iron deposition in cardiac tissue compare to the control group, except the group received  $1 \text{ mg.Kg}^{-1}$  of IONP@CAGQD for one day. Collectively, considering that, administered dose of  $3 \text{ mg.Kg}^{-1}$  for 7 days did not affect the normal architecture of the liver and cardiac tissues, IONP@CAGQD can be offered a potential nanoparticle for nanomedicine applications. However, modifications are needed to improve the toxicity and clearance of these materials.

### 3.4. Potential applications

IONP@CAGQD can be a potential theranostic agent due to its set of properties, including the ability to carry cargo, enhancing the contrast of imaging modalities, and bio-imaging. Some drugs can be loaded onto the surface of GQDs, through  $\pi$ - $\pi$  interactions [3,6]. Moreover, due to the hydrophobic nature of the carbon chains of CA and oleic acid in the middle of IONP@CAGQD, hydrophobic drugs can be loaded in this space [19]. Fluorescent properties of GQDs would also make this hybrid structure suitable for bio-imaging applications (Fig. 3C) [3,6]. Moreover, the Magnetic properties of IONP@CAGQD would make targeting applications possible (Fig. 3b). It has been demonstrated vastly that MNPs can act as contrast agents for MRI or CTscan; therefore, in addition to cargo delivery applications, IONP@CAGQD can be used in imagining contrast enhancement for diagnostic purposes [4]. Moreover, an appropriate function of IONP@CAGQD in biological systems can be tracked through these imaging modalities (Fig. 6). We further hypothesize that relatively loose interaction between IONPs and CAGQDs can be cleaved in response to mechanical stimuli, functioning as a stimuli-responsive theranostic agent [20].

## 4. Conclusion

IONP@CAGQD is composed of CAGQDs as a surfactant, and oleic acid functionalized IONP. In this structure, IONP is located at the center, and it is surrounded by CAGQDs. The successful synthesis of IONP@CAGQD has been approved by XRD, FT-IR, UV-Vis, VSM, and TEM. IONP@CAGQD can be used as a theranostic agent due to its various properties, including hydrophobic and hydrophilic cargo loading abilities, fluorescence, contrast enhancement, targeting abilities, stimuli-responsiveness, and low cytotoxicity.

## References

- [1] V.S. Madamsetty, A. Mukherjee, S. Mukherjee, Recent Trends of the Bio-Inspired Nanoparticles in Cancer Theranostics, *Frontiers in Pharmacology* 10 (2019) 1264.
- [2] H. Huang, J.F. Lovell, Advanced functional nanomaterials for theranostics, *Advanced functional materials* 27 (2017), 1603524.
- [3] K.L. Schroeder, R.V. Goreham, T. Nann, Graphene Quantum Dots for Theranostics and Bioimaging, *Pharmaceutical Research* 33 (2016) 2337–2357.

- [4] V.F. Cardoso, A. Francesco, C. Ribeiro, M. Bañobre-López, P. Martins, S. Lanceros-Mendez, *Advances in magnetic nanoparticles for biomedical applications*, *Advanced Healthcare materials* 7 (2018), 1700845.
- [5] M. Bacon, S.J. Bradley, T. Nann, *Graphene quantum dots, Particle & Particle Systems Characterization* 31 (2014) 415–428.
- [6] A.S. Dezfuli, E. Kohan, S.T. Fateh, N. Alimirzaei, H. Arzaghi, M.R. Hamblin, *Organic dots (O-dots) for theranostic applications: preparation and surface engineering*, *Royal Society of Chemistry* 11 (2021) 2253–2291.
- [7] J. Kudr, Y. Haddad, L. Richtera, Z. Heger, M. Cernak, V. Adam, O. Zitka, *Magnetic nanoparticles: from design and synthesis to real world applications*, *Nanomaterials* 7 (2017) 243.
- [8] F. Xi, J. Zhao, C. Shen, J. He, J. Chen, Y. Yan, K. Li, J. Liu, P. Chen, *Amphiphilic graphene quantum dots as a new class of surfactants*, *Carbon* 153 (2019) 127–135. N Y.
- [9] W. Xuan, L. Ruiyi, L. Zaijun, L. Junkang, *Synthesis of dodecylamine-functionalized graphene quantum dots and their application as stabilizers in an emulsion polymerization of styrene*, *Journal of colloid and interface science* 505 (2017) 847–857.
- [10] H. Yang, K.H. Ku, J.M. Shin, J. Lee, C.H. Park, H.H. Cho, S.G. Jang, B.J. Kim, *Engineering the shape of block copolymer particles by surface-modulated graphene quantum dots*, *Chemistry of Materials* 28 (2016) 830–837.
- [11] H.H. Cho, H. Yang, D.J. Kang, B.J. Kim, *Highly adhesive and soluble polyimide binder: improving the long-term cycle life of silicon anodes in lithium-ion batteries*, *ACS applied materials & interfaces* 7 (2015) 8615–8621.
- [12] L.N. Dinh, L.N. Ramana, V. Agarwal, P.B. Zetterlund, *Miniemulsion polymerization of styrene using carboxylated graphene quantum dots as surfactant*, *Polymer Chemistry* 11 (2020) 3217–3224.
- [13] Zeng M, Wang X, Yu YH, Zhang L, Shafi W, Huang X, Cheng Z. *The synthesis of amphiphilic luminescent graphene quantum dot and its application in miniemulsion polymerization*. *Journal of Nanomaterials*. 2016 Jan 1;2016.
- [14] J. Cai, Y.Q. Miao, B.Z. Yu, P. Ma, L. Li, H.M. Fan, *Large-scale, facile transfer of oleic acid-stabilized iron oxide nanoparticles to the aqueous phase for biological applications*, *Langmuir* 33 (2017) 1662–1669.
- [15] Y. Dong, J. Shao, C. Chen, H. Li, R. Wang, Y. Chi, X. Lin, G. Chen, *Blue luminescent graphene quantum dots and graphene oxide prepared by tuning the carbonization degree of citric acid*, *Carbon* 50 (2012) 4738–4743. N Y.
- [16] J.C. Wood, M. Otto-Duessel, I. Gonzalez, M.I. Aguilar, H. Shimada, H. Nick, M. Nelson, R. Moats, *Deferasirox and deferiprone remove cardiac iron in the iron-overloaded gerbil*, *Translational research* 148 (2006) 272–280.
- [17] J.E. Nelson, L. Wilson, E.M. Brunt, M.M. Yeh, D.E. Kleiner, A. Unalp-Arida, K.V. Kowdley, *Relationship between the pattern of hepatic iron deposition and histological severity in nonalcoholic fatty liver disease*, *Hepatology* 53 (2011) 448–457.
- [18] Y.N. Zhang, W. Poon, A.J. Tavares, I.D. McGilvray, W.C. Chan, *Nanoparticle–liver interactions: cellular uptake and hepatobiliary elimination, controlled release* 240 (2016) 332–348.
- [19] M.H. Hsiao, Q. Mu, Z.R. Stephen, C. Fang, M. Zhang, *Hexanoyl-chitosan-PEG copolymer coated iron oxide nanoparticles for hydrophobic drug delivery*, *ACS macro letters* 4 (2015) 403–407.
- [20] B.G. De Geest, A.G. Skirtach, A.A. Mamedov, A.A. Antipov, N.A. Kotov, S.C. De Smedt, G.B. Sukhorukov, *Ultrasound-triggered release from multilayered capsules*, *Small* 3 (2007) 804–808.